
Since January 2020 Elsevier has created a COVID-19 resource centre with free information in English and Mandarin on the novel coronavirus COVID-19. The COVID-19 resource centre is hosted on Elsevier Connect, the company's public news and information website.

Elsevier hereby grants permission to make all its COVID-19-related research that is available on the COVID-19 resource centre - including this research content - immediately available in PubMed Central and other publicly funded repositories, such as the WHO COVID database with rights for unrestricted research re-use and analyses in any form or by any means with acknowledgement of the original source. These permissions are granted for free by Elsevier for as long as the COVID-19 resource centre remains active.

Journal of Membrane Science 661 (2022) 120885

Contents lists available at ScienceDirect

Journal of Membrane Science

journal homepage: www.elsevier.com/locate/memsci

# Biocompatible curcumin coupled nanofibrous membrane for pathogens sterilization and isolation

Yuanyuan Rao [a], Shasha Feng [a], Ze-Xian Low [a,b], Junwei Wu [a,c], Shengui Ju [a], Zhaoxiang Zhong [a,*], Weihong Xing [a]

[a] State Key Laboratory of Materials-Oriented Chemical Engineering, National Engineering Research Center for Special Separation Membrane, Nanjing Tech University, Nanjing, 210009, China
[b] Department of Chemical and Biological Engineering, Monash University, Clayton, VIC, 3800, Australia
[c] Jiangsu Jiulang High-Tech Co., Ltd, Nanjing, 210009, China

ARTICLE INFO

*Keywords:*
Curcumin
PTFE nanofiber Membrane
Antibacterial and antiviral activity
Protective equipment
Pandemic pathogens

ABSTRACT

Airborne transmission of pathogens is the most probable cause for the spread of respiratory diseases, which can be intercepted by personal protective equipment such as masks. In this study, an efficient antiviral personal protective filter was fabricated by coupling the biocompatible curcumin (CCM) with nanofibrous polytetrafluoroethylene (PTFE) membrane. The CCM extracted from plants was first dissolved in acidified ethanol at a certain pH and temperature to optimize its loading concentration, antiviral activation, and binding forces on the polyethylene terephthalate (PET) support to form a pre-filtration layer at the front section of the filter. Ultrathin PTFE membrane was then fabricated on the antibacterial-antiviral PET support (A-A PET) by controllable heating lamination. This functional layer of the filter exhibits good gas permeance (3423.6 $m^3/(m^2 \cdot h \cdot kPa)$) and ultrafine particles rejection rate (>98.79%). Moreover, the obtained A-A filter exhibit a high antibacterial rate against a variety of bacteria (*E. coli, B. subtilis, A. niger,* and *Penicillium* were 99.84%, 99.02%, 93.60%, 95.23%, respectively). Forthwith virucidal (SARS-CoV-2) efficiency of the A-A filter can reach 99.90% for 5 min. The filter shows good stability after 10 heating cycles, demonstrating its reusability.

## 1. Introduction

The transmission of pathogens attached to aerosols and droplets may promote the spread of airborne diseases [1,2]. Personal protective equipment like face masks can effectively prevent the infection from airborne pathogens, which has been demonstrated in the COVID-19 pandemic [3,4]. Meltblown fibers with large void space and electrostatic storage capacity are widely used in masks for its effective physical barrier and high gas permeance [5]. However, the electrostatic storage capacity could be degraded during consecutive donning and disinfection treatments, leading to a concomitant drop in the filtration capacity during use [6]. Further, improper disposal of used masks often causes serious environmental problems and waste of resources [7,8], More significantly, using masks incorrectly can cause severe cross-infection, and secondary transmission [9,10]. Therefore, a low toxicity, reusable and highly effective antiviral protective material is urgently needed.

Organic nanofibrous membranes such as polyimide (PI), polyurethane (PU), polyacrylonitrile (PAN), polyamide-66 (PA-66), and polytetrafluoroethylene (PTFE) etc. [11–13], are the ideal materials for ultrafine particle filtration due to their unique nanostructures, which have been employed in the design of respirator mask alternative to melt-blown fabrics [14]. Among them, biaxial stretched PTFE membrane with continuous nodes connected nanofibers possesses better structural stability and antifouling property in air cleaning process [15].

To endow the membrane with pathogen sterilization property, many researchers have focused on loading antibacterial or antiviral composite on the membrane via post-treatment [16]. However, the basic properties of nanofiber-constructed substrate may be significantly impacted during the modification process, leading to poor filtration efficiency and gas permeance. In addition, as the last barrier for particulate matters (PMs), the nanofiber membrane may not completely intercept the particles, and the minor contact area and contact time between the porous nanofibrous membranes (NFMs) and virus may not effectively eliminate the virus/-bacteria, leading to potential infection risk [17]. Therefore, capturing and sterilizing the hazardous matters before the filtration layer is necessary in the design of antibacterial-antiviral functional filter (A-A

* Corresponding author.
*E-mail address:* zhongzx@njtech.edu.cn (Z. Zhong).

https://doi.org/10.1016/j.memsci.2022.120885
Received 30 May 2022; Received in revised form 19 July 2022; Accepted 29 July 2022
Available online 10 August 2022
0376-7388/© 2022 Elsevier B.V. All rights reserved.

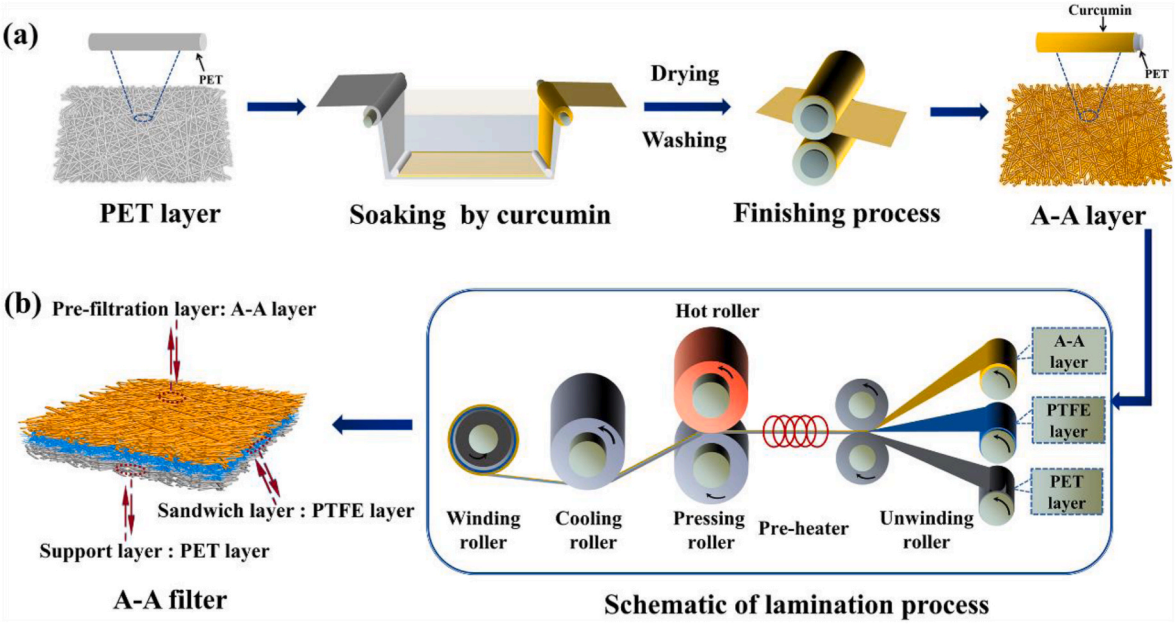


**Fig. 1.** Schematic illustration of the preparation process for (a) A-A layer and (b) A-A filter.

filter).

Antimicrobial technologies that use physical or chemical methods by incorporating biocidal agents to provide bio-protection against pathogens can be effective if killing of pathogens by direct contact can be achieved. At present, the biological agents used in the biological protection materials mainly include natural antibacterial agents and artificial antibacterial agents. Previous studies have reported that various antimicrobial materials, such as silver (Ag) [18,19], copper (Cu) nanoparticles [20], and carbon nanotubes (CNTs) [21], are effective in controlling bioaerosols. These materials have been used to engineer the antimicrobial functionality to air filtering media. However, concerns remain on the potential health risk of exposure to inorganic nanoparticles, leading to the study of antimicrobial alternatives such as food-grade compounds [22].

Curcumin (CCM) extracted from the turmeric has attracted much attention due to its broad-spectrum biological actions. It shows a remarkable range of pharmacological activity, including antioxidant [23], antitumor [24], wound healing [25], and antifungal [26]. CCM exhibits inhibitory ability against the proliferation of diverse bacteria and viruses [27,28]. It is worth noting that CCM shows great applicability in materials modification due to its low toxicity, high antimicrobial activity, mild environmental effects, and low cost.

Herein, a biocompatible curcumin-incorporated composite membrane was fabricated by A-A functionalization and controllable hot lamination for efficient pathogens sterilization and isolation. The PET nonwoven fabric was firstly A-A functionalized with plant-extracted CCM. The A-A efficiency of CCM were systematically optimized in the loading and heat laminating processes, respectively. The A-A support coupled filter exhibits superior aerosol filtration and rapid antibacterial and antivirus property with good biocompatibility and reusability.

## 2. Experimental

### 2.1. Materials

Curcumin (>98%) was purchased from Sinopharm Chemical Reagent Co. Ltd., China. Gram-negative *Escherichia Coli* (*E. coli*, ATCC 25922), Gram-positive *Bacillus subtilis* (*B. subtilis*, CMCC 63501), Fungus *Penicillium* (A S 3.4042) and Fungus *Aspergillus niger* (*A. niger*, A S 3.3928) were purchased from the Center for Conservation Biotechnology in Shanghai, China. Lysogeny broth (LB), Bengal red medium (BRM), Potato Dextrose Agar Medium (PDA), and phosphate-buffered saline (PBS) were purchased from Thermo Fisher Scientific, America. Soya casein digest lecithin polysorbate (SCDLP) were purchased from Cyclokay Microorganism, China. Propidine iodide (PI), and SYBR Green (SG) dye were purchased from Sigma-Aldrich. Porous PTFE membrane and PET non-woven fabric were obtained from Jiangsu Jiulang High-Tech Co., Ltd, China. KN95 Particulate Respirator was purchased from Zhengzhou Wanshenshan Healthcare PPE Co., Ltd, China. Single-use medical face mask was purchased from Zhende medical supplies Co., Ltd, China. The African green monkey kidney cell (Vero-E6) and Dulbecco's Modified Eagle Medium (DMEM) were obtained from Jiangsu Provincial Center for Disease Control and Prevention, China. All other chemicals were purchased from Sinopharm Chemical Reagent Co. Ltd., China, and used without further purification. Water used in all experiments was purified by deionization.

### 2.2. Characterization

The morphology of the membranes and microorganisms was observed by field emission scanning electron microscopy (FESEM, Hitachi S-4800). The gas permeability and average pore size of the membranes were measured by a capillary flow porometer (PMI, ipore-1500) under $N_2$ atmosphere. Galwick (surface tension 15.9 mN/m) was selected as the wetting fluid. The chemical structure was confirmed with the attenuated total reflection (ATR) method by Fourier Transform infrared spectroscopy (FT-IR, Nicolet 8700). The crystal structure was determined using an X-ray diffractometer (XRD, Rigaku MiniFlex 600). Contact-angle measurement was performed on a contact angle goniometer (Dropmeter A-100). The average contact angle was obtained by measuring the contact angle of the liquid droplets (5 μL) on three different areas of the material surface.

### 2.3. Preparation of A-A filter

The A-A filter was obtained by compositing the CCM loaded PET layer and the effective PTFE separation layer via thermal laminating process. At first, 0.4 g CCM was dispersed in 1 L distilled water. Acidified ethanol (i.e., 0.5 mol/L ethanol and 1.0 mol/L acetic acid were mixed at a ratio of 21:4 (v/v)) and 0.1 mol/L of citrate buffers were added in the

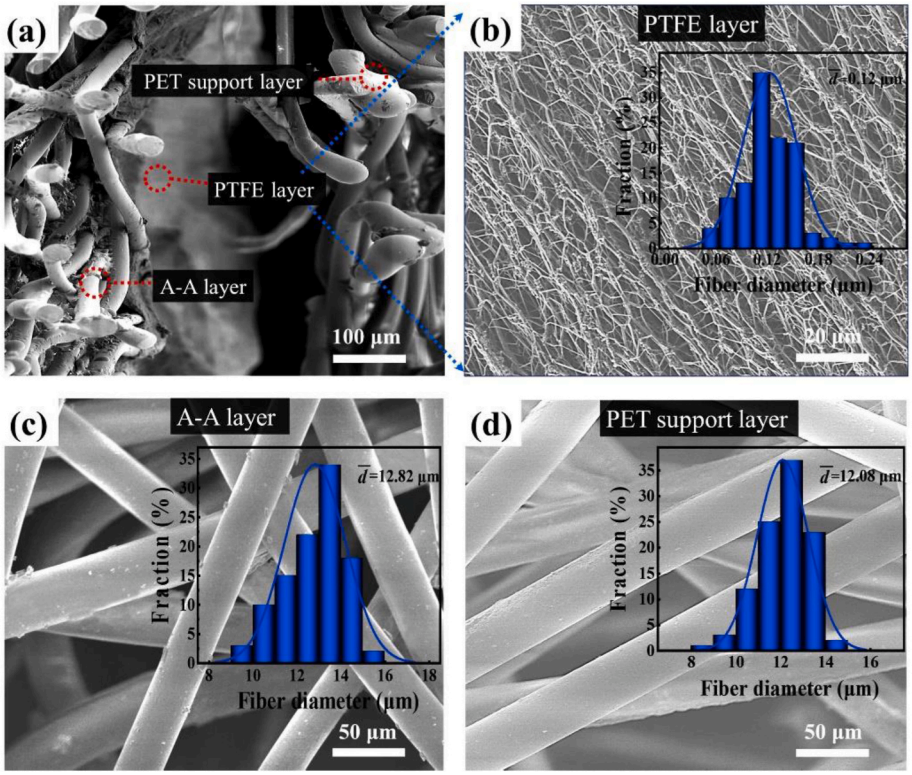


**Fig. 2.** (a) Cross-sectional SEM image of an A-A filter showing that the filtration layer is composited between the supportive layers. SEM images of (b) PTFE layer, (c) A-A layer, (d) PET support layer.

dispersion to dissolve the CCM and adjust the solution pH (4-10). Then, the initial PET layer was impregnated in different temperatures (50–120 °C) of CCM mixed solution via a home-made dyeing machine for 0.5 h. After being washed and dried, the CCM on the PET support layer was further strengthened by continuous-rolling mill to prepare the A-A layer, as shown in Fig. 1a.

The laminating process of A-A filter was carried out according to our previous work [29]. The lamination equipment was obtained and customized from Lvhuan Machinery Co., Ltd., China. The hot roller was heated to the required temperature and stabilized for 30 min. The A-A PET, PTFE nanofiber membrane and PET support were preheated in an infrared oven. The laminating pressure (100 Pa) and speed (2 m/min) were selected by controlling the pressing roller and winding roller, respectively. The A-A filter was then collected by the winding roller after cooling at room temperature. as shown in Fig. 1b.

### 2.4. Filtration performance evaluation

The particle sizer spectrometer (TSI, SMPS-3938) was employed to test the removal efficiency for NaCl aerosols (2 wt%) with diameter ranging from 0.3 μm to 10 μm. During the filtration test, the effective area of filter was controlled at 25 $cm^2$ at a gas velocity of 10.66 cm/s. The effect of different gas velocities (5.33, 21.32, 42.64 cm/s) on filtration performance was tested under the same conditions. Each average measurement contains at least three individual sample measurements. The quality factor ($Q_f$, $Pa^{-1}$) was calculated as [30]:

$$Q_f = -\ln(1-\eta)/\Delta P \quad (1)$$

where $\eta$ (%) represents the PM removal efficiency and $\Delta P$ represents the pressure drop.

The penetrated NaCl aerosol particles were generated and counted via the filter performance tester (Huada, LZC-K1). Samples with an effective area of 12.56 $cm^2$ were clamped in the tube module for testing. The gas velocity was controlled at 5.33 cm/s. The concentration of NaCl aerosol was controlled by the aerosol generator while particle sizer spectrometer was used to evaluate the filtration efficiency of the samples. The integral area of the particles before and after filtration were calculated to evaluate the particles interception rate (R) [31]:

$$R = \left(1 - \frac{\sum_{10}^{1000} \frac{4}{3}\pi\left(\frac{D}{2}\right)^3 \rho N_{outlet}}{\sum_{10}^{1000} \frac{4}{3}\pi\left(\frac{D}{2}\right)^3 \rho N_{inlet}}\right) \times 100 \quad (2)$$

where $\rho$, D, and N are the density, diameter, and number of the aerosol, and 10 and 1000 represent the diameters of NaCl aerosol in nm. The particle interception rate can be measured by the apparatus in the range of 10–1000 nm.

### 2.5. Antibacterial activity assay of filter

Appropriate concentrations of bacterial and fungal suspensions were prepared for antibacterial experiments (Supporting Information S1). For the static antibacterial experiments, the filters were cut into square specimens with a diameter of 40 ± 5 mm, and four parallel specimens were made for each strain. 1 mL test bacterial solution was added into the 15 mL of agar medium, and allowed to coagulate. Samples were placed in the center of the plate with sterile tweezers to have a full contact between the sample and the agar medium. Then, the samples were put into incubator at 37 ± 2 °C (fungi, 28 ± 2 °C) for 18–24 h (fungi, 36–48 h). Blank (only bacteria suspension) and commercial filters were also treated as controls for comparison.

For the dynamic antibacterial experiments, bacterial droplets were generated by a single-jet collision nebulizer, which deposited on the A-A filters and commercial filters (40 ± 5 mm in diameter) for 5 min. Then, the tested filters were covered with a non-antibacterial filter to maintain proper contact between the surface of the test filter and the bacteria for 2 h. Subsequently, the morphology of bacteria on the filter was observed

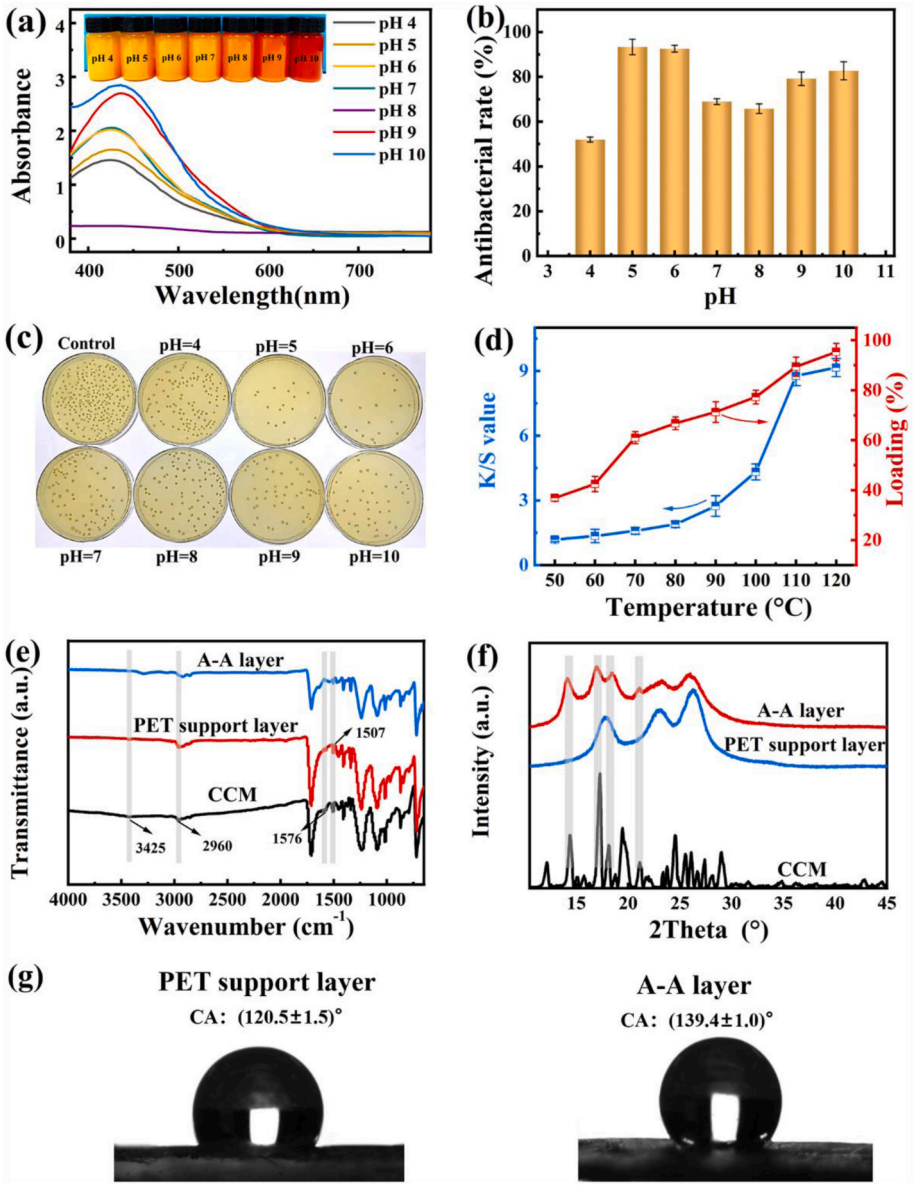


**Fig. 3.** (a) Visible spectra of CCM and (b) Antibacterial rates and (c) Photographs of *E. coli* colonies at different pH values. (d) K/S value and loads of A-A layer at different temperatures (Concentration of CCM was 0.4 g/L, the area of A-A layer was 25 $cm^2$). (e) FT-IR spectra, (f) XRD patterns of the PET support layer, A-A layer, CCM powder. (g) Digital photographs of water contact angle on PET support layer and A-A layer.

by electron microscope. Simultaneously, the test filters (including cover filter) and sterile water were added immediately into the vials. Then the vials were agitated by vortex mixer for 5 s and 5 times for washing out the bacteria or fungi from the test filters. The bacteria suspension from the test filters was diluted serially with sterile water and plated on a nutrient broth agar. The antibacterial rates of the filters for bacteria and fungi were assessed according to the following equation [32,33]:

$$R_{bacterial}(\%) = \frac{A-B}{A} \times 100 \quad (3)$$

where A is the number of live bacteria in the original bacteria suspension and B is the number of live bacteria on the test filters surface.

### 2.6. Circulating filtration and antibacterial performance

Samples were heated in an 80 °C oven for 30 min to test their filtration and antibacterial stability, respectively. After each treating cycle, the NaCl aerosols filtration performance and antibacterial performance for *E. coli* were evaluated.

## 3. Results and discussion

### 3.1. Morphology analysis

The cross-sectional electron microscopy of A-A filter is composed of A-A layer, PTFE layer, and PET support layer (Fig. 2a). The PTFE nanofiber interlace to form a three-dimensional spider web structure and the average diameter of the nanofibers was 0.12 μm (Fig. 2b). The high specific surface area and fine fibers of PTFE membrane provide more opportunities for aerosol capture [34]. The average fiber diameter of the PET support layer was 12.08 μm (Fig. 2d). After immersing in a high-temperature curcumin solution, the average fiber diameter of A-A increased slightly to 12.82 μm (Fig. 2c).

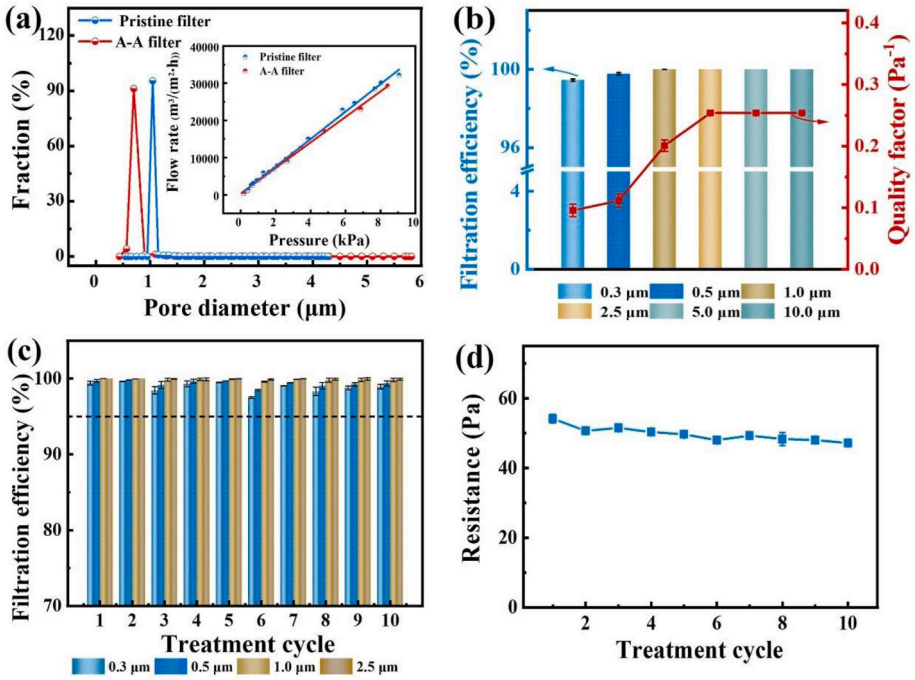


**Fig. 4.** (a) Pore sizes and gas permeability of pristine filter and A-A filter. (b) NaCl aerosols filtration efficiency and quality factor of A-A filter. (c) Filtration efficiency and (d) Resistance of A-A filter after each heat treatment.

### 3.2. Crystal structure and surface physicochemical analysis

The antibacterial activity of the composited CCM is related to the solution pH [35]. CCM has been found to possess pH-dependent solubility, which exhibits different colors at different pH values (Fig. 3a) [36]. These changes were due to the reversible structural transformation of CCM at different pH (Fig. S1) [37]. When the pH was below 8, the maximum absorption peak was around 425 nm. With the increase of pH, the maximum absorption wavelength of CCM shifted from 425 nm to 438 nm. To further verify the bacteriostatic effect under different pH, a certain concentration of bacterial and CCM solution were mixed (Supporting Information S2). The antibacterial rates (Fig. 3b) and photographs of *E. coli* colonies (Fig. 3c) showed that the antibacterial effect was the most significant when the pH was controlled at 5, where the antibacterial rate of *E. coli* reached 95.31%.

The bonding force between PET support and CCM is closely related to temperature and can be reflect by the K/S value (Fig. 3d). The K/S value of the Kubelka-Munk equation was applied to the change in color of the sample, which verifies the fastness of the sample at different temperatures (Supporting Information S3). The K/S value has an exponential growth from 50 °C to 120 °C, demonstrating higher temperature resulting in better fastness of CCM. Also, the CCM loading amounts showed a positive correlation to the temperature with an 80% more of CCM at the treating temperature above 110 °C.

Fourier transform infrared spectroscopy (FT-IR) is used to explore the chemical structure of the material and to obtain relevant information about the functional groups contained in the CCM, PET support layer and A-A layer (Fig. 3e). Compared with the PET support layer, the A-A layer has two clear peaks at 2960 $cm^{-1}$ and 1576 $cm^{-1}$, which are formed by the deformation and vibration of benzene ring in the CCM structure, and the characteristic absorption peak at 1507 $cm^{-1}$ stem of CCM indicates that CCM exists in the A-A layer [38]. In the FT-IR spectrum of the A-A layer, the peak at 3501 $cm^{-1}$ corresponds to the phenolic hydroxyl telescopic vibration peak, which is derived from the characteristic peak of CCM. These results showed that CCM was well integrated in the PET support layer. The effect of temperature on the elements on the A-A layer were also investigated, and it was found that no new substances were produced (Fig. S2a).

Fig. 3f shows the X-ray diffraction patterns of CCM, PET support layer and A-A layer in the 2θ range of 5-50°. The crystal peaks of CCM are narrow and sharp, indicating the presence of CCM in crystalline form [39]. The X-ray diffraction patterns of the PET support layer show dispersive and broad diffraction peaks at 17.8°, 23° and 26.2°, which are independent of the crystal structure. In the XRD pattern of A-A layer, the diffraction peaks of CCM at 14.3°, 17.1°, 18.2°, and 21.2° indicate that CCM has been successfully loaded on the PET support layer.

The hydrophobicity of PET support layer, and A-A layer were determined by water contact angle (WCA) measurements (Fig. 3g). The PET non-woven fabric has no other polar groups except the two alcohol-terminated hydroxyl groups in the molecule, which has a hydrophobic surface with a WCA of 120.5 ± 1.5°. The A-A layer also exhibited hydrophobic properties by loading the hydrophobic CCM. At increasing temperature, the contact angle of the A-A layer shows an increasing trend (Fig. S2b). When the temperature reaches 120 °C, A-A layer shows strong ability to repel water droplets, where the contact angle of 139.4 ± 1.0° was recorded.

### 3.3. Filtration performance evaluation

The breathability of the A-A filter is vital for its practical application [40], which was evaluated by WVTR (Supporting Information S4). As shown in Fig. S3, the pristine filter exhibited higher WVTR of 11.389 kg $m^{-2}$ $d^{-1}$. After compositing with A-A layer, the WVTR of A-A filter was slightly decreased to 10.651 kg $m^{-2}$ $d^{-1}$. The reduction of WVTR can be explained by the increase of hydrophobicity [41]. Nevertheless, the breathability of the A-A filter is still higher than that of disposable medical face mask (C-SMFA, 9.782 kg $m^{-2}$ $d^{-1}$) and KN95 particulate respirator (C–KN95, 9.188 kg $m^{-2}$ $d^{-1}$).

Fig. 4a is the pore size distribution diagram of the pristine filter and the A-A filter. The average pore diameter of the pristine filter and the A-A filter was 1.03 μm and 0.73 μm, respectively. The decrease in the pore diameter resulted in a slight reduction in gas permeance of the A-A filter (3423.6 $m^3/(m^2 \cdot h \cdot kPa)$) compared to that of pristine filter (3695.1 $m^3/(m^2 \cdot h \cdot kPa)$). The filtration efficiency and quality factor revealed that A-

**Table 1**
PM filtration performance comparison of this work and other filters.

| Materials | Air flow velocity (cm/s) | Particulate matters (μm) | Filtration efficiency (%) | Pressure drop (Pa) | Quality factor ($Pa^{-1}$) | Reference |
|---|---|---|---|---|---|---|
| CCM/PTFE/PET | 5.33 | 0.3–2.5 | >99.45 | ~54.24 | >0.095 | This work |
| ATTM/PAN | 5 | 0.3 | 99.626 | 184.27 | ~0.03 | [44] |
| Cellulose filter II | ~0.115 | 0.05–0.5 | 98.76 | 2100 | 0.0026 | [45] |
| $MnO_2$@ZnO@PP | 14.1 | 2.5, 10.0 | >99.5 | ~60 | ~0.036 | [46] |
| PTFE/Nylon | ~4 | 0.3–0.5 | 84.7 | ~104.30 | ~0.02 | [47] |

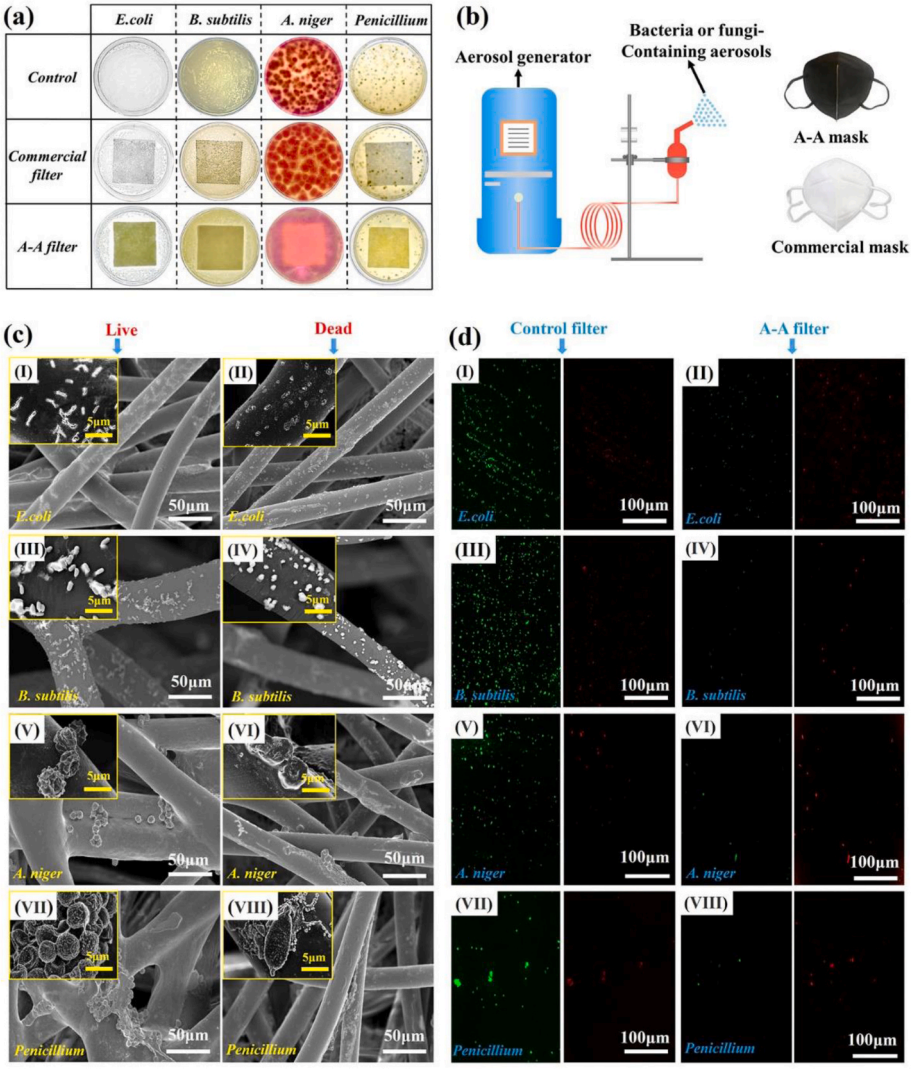


**Fig. 5.** (a) Optical photographs showing the results of inhibition zone test in A-A or commercial filter against *E. coli*, *B. subtilis*, *A. niger*. *Penicillium*. (b) Bacterial and fungi aerosol generation, the interception test by A-A or commercial mask. (c-d) Morphology and live/dead bacterial viability assay of c (I, II)-d (I, II) *E. coli,* c (III, IV)-d (III, IV) *B. subtilis,* c (V, VI)-d (V, VI) *A. niger*, c (VII, VIII)-d (VII, VIII) *Penicillium* in contact with control filter and A-A filter for 2 h.

A filter exhibits a high $PM_{0.3}$ filtration efficiency of 99.45% with the quality factor of 0.095 $Pa^{-1}$ (Fig. 4b). For PM diameter larger than 2.5 μm, the filtration efficiency reaches 100% with a higher quality factor value of 0.297 $Pa^{-1}$. Table 1 compares the PM filtration efficiency and quality factor of the A-A filter and other reported filters. A-A filter has better $PM_{0.3}$ filtration efficiency (99.80%) at a higher gas velocity of 42.64 cm/s, and a more prominent $PM_{0.3}$ quality factor (0.14 $Pa^{-1}$) at a lower gas velocity of 5.33 cm/s (Fig. S4 (a, b)). The outstanding quality factor of the A-A filter can be attributed to the nanofiber structure of PTFE membrane. The diameter of PTFE fibers can be controlled comparable with the mean free path of the air molecules (66 nm under normal conditions), which results in a non-zero of gas velocity on the nanofiber surface due to the "slip" occurs [42]. It significantly reduces the drag force of gas flow which resulting in a lower filtration resistance.

The reusability of A-A filter upon heat disinfections in 10 treatment cycles, and the corresponding results of filtering performance after each treatment are illustrated in Fig. 4c and d. We observed little change in the filtration properties. After 10 cycles of heat disinfection treatments, the filtration efficiency of all $PM_s$ can be maintained stable over 95% (only about ~0.52% reduction for $PM_{0.3}$). The slightly decreased filtration efficiency can be attributed to the microstructure change of the membrane after heating treatment (Fig. S5). The filtration efficiencies of $PM_{5.0}$ and $PM_{10.0}$ were maintained at 100% consistently (Fig. S6). In addition, the pressure drop remains comparable stability along with the

**Table 2**
Antibacterial rates of A-A filter against bacteria and fungi.

| Strain | Number of live bacteria in the original bacteria suspension (CFU/mL) | Number of live bacteria on the test filters surface (CFU/mL) | Antibacterial rate (%) |
|---|---|---|---|
| *E. coli* | $2.6 \times 10^5$ | $4.0 \times 10^2$ | 99.84 |
| *B. subtilis* | $4.3 \times 10^5$ | $4.2 \times 10^3$ | 99.02 |
| *A. niger* | $2.5 \times 10^4$ | $1.6 \times 10^3$ | 93.60 |
| *Penicillium* | $6.3 \times 10^4$ | $3.0 \times 10^3$ | 95.23 |

heat treatment cycles (decline 7.25 Pa). This can effectively reduce the risk of particle inhalation by reusing the filter after undergoing disinfection processes [43].

### 3.4. Antibacterial effects of A-A filter

The A-A filter, as an internal germicidal layer of face mask between the non-woven layer and hot air cotton layer, was prepared to evaluate its practical antibacterial activity. The A-A mask was assessed by comparison with a commercial mask. As demonstrated in Fig. 5a, a large amount of *E. coli, B. subtilis, A. niger* and *Penicillium* adheres on the surface of commercial mask and forms a bacterial biofilm. On the other hand, very few bacteria appeared on the A-A filter, especially the *E. coli, B. subtilis and Penicillium*. An inhibition zone was also observed around the A-A filter.

The internal filter layer of the mask was exposed to artificial pathogenic aerosols generated from suspensions (Fig. 5b). Table 2 shows that the antibacterial rates of A-A filter against *E. coli*, *B. subtilis, A. niger* and *Penicillium* were 99.84%, 99.02%, 93.60%, 95.23%, respectively. The morphology of the four types of microorganisms in this experiment changed greatly after contacting the A-A filter. Fig. 5c (I, III, V, VII) shows the microbial cells having a complete structure on the pristine filter. *E. coli* and *B. subtilis* showed a typical rod shape, *A. niger* and *penicillium* showed a convex round shape. It can be seen from Fig. 5c (II, IV, VI, VIII) that the cell structure was destroyed, indicating the A-A filter has good antibacterial performance. It has been previously demonstrated that the CCM can cause rupture of the cell wall, leading to cell content leakage [48]. Meanwhile, the hydrophobic A-A filter can potentially induce dehydration for a bacterium, leading to its inhibition [17]. Therefore, CCM and hydrophobic features of filter create an enhanced effect that provides stronger protection against bacteria and viruses.

To further verify the live/dead state of bacteria and fungi after contact the control filter and the A-A filter (Supporting Information S5). As shown in Fig. 5d, numerous live *E. coli*, *B. subtilis*, *A. niger*, *Penicillium* were observed in green color after contacting the control samples, with a small proportion in red, representing few dead bacteria. In contrast, upon 1 h of contact with the A-A filter, the observed green fluorescence signals were significantly decreased. Almost all cells were stained in red color, revealing that most bacterial cells were disrupted or lysed without any integrated morphology [49].

The antibacterial rates of A-A filter on *E. coli* could still be maintained over 97.56% after 10 heat treatment cycles (Fig. 6a). K/S value of the A-A filter remained unchanged, which was consistent with the antibacterial results (Fig. 6b). The results suggested that the A-A layer prepared at high temperature with CCM has strong bonding force, confirming the experimental results in Fig. 3.

To verify the long-lasting antibacterial effect of A-A filter, the A-A filter was folded and put into an air purifier to test its antibacterial properties with *E. coli* after using it for a period of time. The results showed that the antibacterial rates of A-A filter against *E. coli* could still reach 98.25%, 96.75% and 88.75% after 1 month, 3 months and 6 months, respectively (Fig. 6c). Two orders of magnitude reduction can be seen from the photographs of *E. coli* colonies (Fig. 6d). CCM has better solubility and stability after being treated with a certain amount of acetic acid and ethanol. Not only can the interaction between the CCM

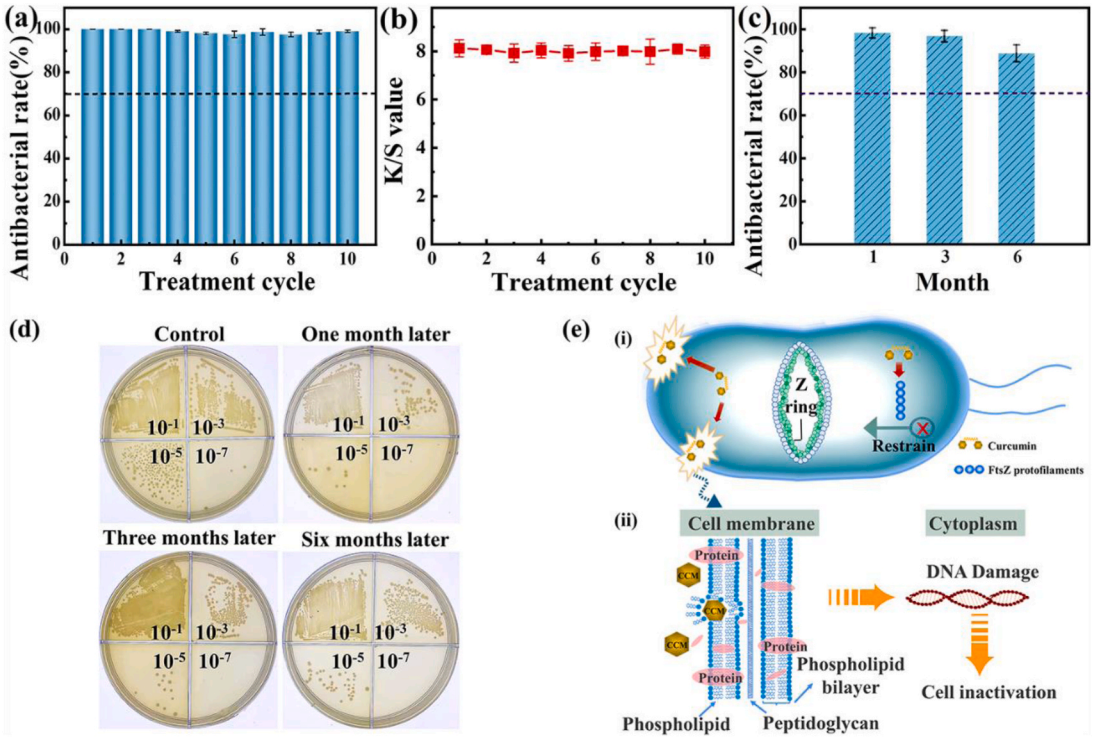


**Fig. 6.** (a) Antibacterial rates and (b) K/S value of A-A filter after 10 heat treatment cycles. (c) Antibacterial rates and (d) Photographs of *E. coli* colonies treated by A-A filter after using one month, three months and six months, respectively. (e) Antibacterial mechanisms of CCM. (i) CCM with inhibitory activity, prevents Z-ring formation by inhibiting the assembly of FtsZ. (ii) CCM causes disturbance of lipid membranes and damage to genetic information, ultimately resulting in bacterial cell death or viral inactivation.

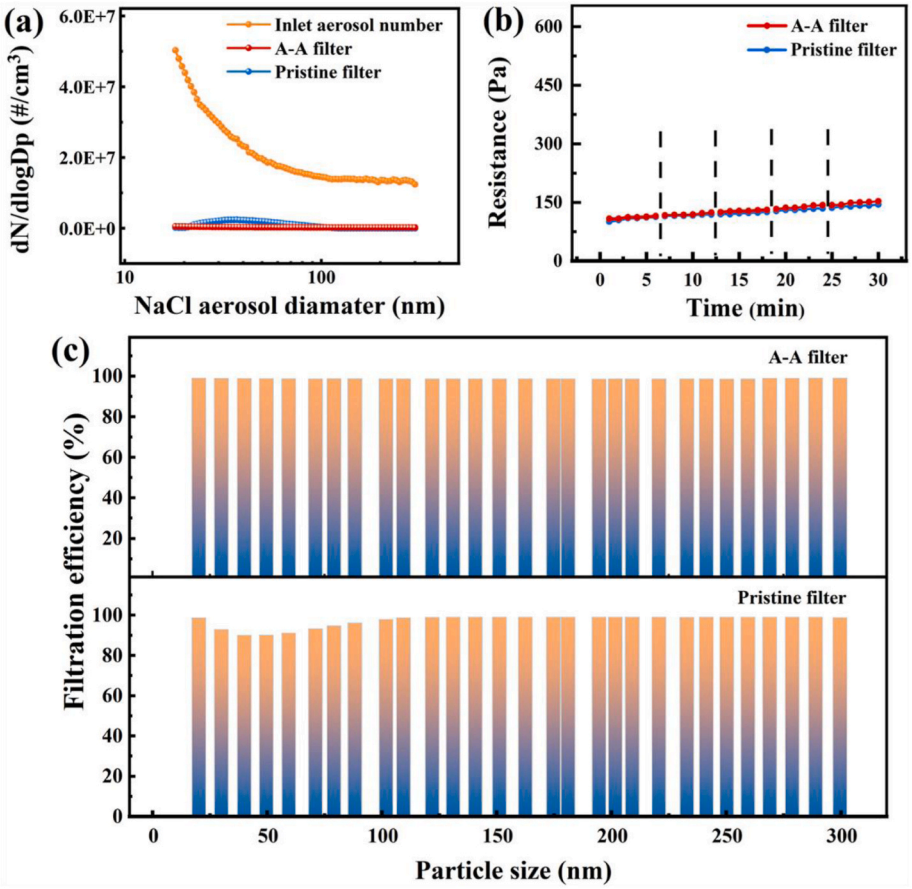


**Fig. 7.** (a) The counts of the NaCl aerosols with different diameter before and after filtration. (b) The pressure drop and (c) Filtration efficiency of pristine filter and A-A filter, respectively.

and PET layers be stabilized, but the antibacterial activity of the A-A filter is also enhanced, giving the A-A filter a great reusability potential under harsh conditions.

Four major routes of antimicrobial action for CCM are provided, (i) adhesion to cell membrane, (ii) effect on proteins, (iii) phototoxicity and ROS generation, and (iv) penetration inside the cell and nucleus (Fig. S7). CCM inhibiting the assembly dynamics of filamentous temperature-sensitive protein Z (FtsZ) in the Z-ring is the most important antibacterial mechanisms, which destroys the proliferative division of bacterial cell to achieve antimicrobial activity (Fig. 6e(i)) [50]. The stability and assembly of FtsZ protofilaments is a crucial factor for bacterial cytokinesis. When the CCM interacts with the active site of FtsZ, the binding ability of FtsZ protofilaments is weakened. Simultaneously, curcumin can inhibit bacterial biofilm formation and prevent the bacterial adhesion to host receptors, ultimately resulting in bacterial cell death or inactivation (Fig. 6e(ii)) [51].

### 3.5. Virus filtration and antiviral performance

Particulates with a diameter under 0.3 μm are more difficult to capture due to their teeny sizes, which is similar in size to the virus [6]. For example, the dimensions of the picornaviruses are around 30 nm and the mean diameter of influenza viruses is approximately 120 nm. Therefore, 18–300 nm NaCl aerosol size were used to simulate the virus in this experiment (Fig. 7a). The initial pressure drops of pristine filter and A-A filter were 101 Pa and 108 Pa, respectively. After 30 min filtration test, the increase in the pressure drop for the pristine filter and the A-A filter was 30.34% and 29.41%, respectively (Fig. 7b). The NaCl aerosol filtration performance demonstrated that both pristine filter and A-A filter can effectively intercept the aerosols (Fig. 7c). However, the A-A filter has a better filtration efficiency at the most penetrating particle size (the NaCl aerosol size is 40 nm), which was 98.79%, while the pristine filter was only 90.05%.

The cytotoxicity of the pristine filter and the A-A filter for Vero-E6 cells was tested (Supporting Information S6). Morphological study of Vero-E6 cells revealed the cells undergo an important change in shape and dimensions at different concentrations of A-A filter (Fig. S8a). The A-A filter-0.4 was cytotoxic towards Vero-E6 cells at concentrations of up to 0.4 g/L. Moreover, pristine filter and A-A filter-0.04 showed no cytotoxicity to Vero-E6 cells, although A-A filter-0.1 were moderately

**Table 3**
Antiviral activity of A-A filter against SARS-COV-2.

| Samples | CT value of control filter | | | | CT value of A-A filter | | | | Virus inhibition rate(%) |
|---|---|---|---|---|---|---|---|---|---|
| | 1 | 2 | 3 | 4 | 1 | 2 | 3 | 4 | |
| 1 | 40.00 | 40.00 | 35.90 | 40.00 | 19.51 | 18.87 | 18.66 | 18.57 | >99.90% |
| 2 | 40.00 | 35.85 | 40.00 | 36.24 | 18.68 | 18.42 | 19.18 | 19.9. | >99.90% |
| 3 | 40.00 | 35.99 | 36.18 | 35.57 | 19.40 | 19.10 | 18.76 | 19.41 | >99.90% |

Note: CT = 40 represents no gene amplification.

cytotoxic. Therefore, A-A filter-0.04 was chosen to antiviral experiments, which did not reduce the cell sensitivity to virus and inactivation of antiviral activity.

The antiviral test was based on the relevant operating technical specifications of the new coronavirus (SARS-CoV-2) live virus in the BSL-3 laboratory of the Jiangsu Provincial Center for Disease Control and Prevention, meanwhile, the antiviral activity of textile products (BS ISO 18184–2019) was referenced (Supporting Information S7). The inhibition rate of SARS-CoV-2 virus activity is greater than 99.90%, which was evenly spread on the A-A filter-0.04 for 5 min (Table 3). CCM is a plant-derived polyphenolic active substance which can be used to damage the amino (-$NH_2$) and carboxyl (-COOH) groups of RNA in the coronavirus [52]. Ultimately, the process of viral adsorption, entry, replication and even budding were disrupted to the inactivation of the SARS-CoV-2 [53] (Fig. S8b).

## 4. Conclusion

In summary, a biological extracted CCM was introduced to fabricated an antibacterial and antivirus membrane by nondestructive thermal laminating composite technology. This functionalized membrane can simultaneously intercept and sterilize pathogens such as bacteria and virus. CCM loading condition, including the dose, pH and temperature that closely relevant to its biological activities and binding force to the substrate were optimized combining the membrane heating laminating parameters. The obtained membrane exhibits high gas permeance of 3423.6 $m^3/(m^2 \cdot h \cdot kPa)$, and up to 98.79% of interception rate to 18–300 nm NaCl aerosol particles. A-A filter has superior antibacterial activity against Gram-negative (*E. coli*), Gram-positive bacteria (*B. subtilis*) and fungus (*A. niger, Penicillium*) in short time (5 min) with long-lasting and effective antibacterial properties after 6 months of use. The reusability of the A-A filter can be effectively embodied in high temperature disinfection cycles at 80 °C, which is significant for circular economy and environmental protection. This work supplies a facile and efficient way to functionalize the filter with antibacterial and antivirus roles, combining the efficient aerosol filtration performance, which can be effectively applied to personal and public protection.

## Author statement

**Yuanyuan Rao:** Conceptualization, Methodology, Formal analysis, Investigation, and Writing - Original Draft.

**Shasha Feng:** Methodology, Formal analysis, Writing - Review & Editing.

**Ze-Xian Low:** Methodology, Formal analysis, Writing - Review & Editing. **Junwei Wu:** Methodology, Writing - Review & Editing.

**Shengui Ju:** Writing - Review & Editing, Funding acquisition.

**Zhaoxiang Zhong:** Conceptualization, Methodology, Writing-Review & Editing, Supervision, Funding acquisition.

**Weihong Xing:** Conceptualization, Review & Editing, Supervision, Funding acquisition.

## Declaration of competing interest

The authors declare that they have no known competing financial interests or personal relationships that could have appeared to influence the work reported in this paper.

## Data availability

Data will be made available on request.

## Acknowledgments

Financial support was provided by the National Key R&D Program (2021YFB3801302), the National Key R&D Project of China (2018YFE0203500), the National Natural Science Foundation of China (21921006, 21878148), the Key Industrial R&D International Cooperation Project (BZ2018004), and the Key R&D Program of Jiangsu Province (BE2019117). Thanks are due to Jiangsu Provincial Center for Disease Control and Prevention for assistance with the test of SARS-CoV-2.

## Appendix A. Supplementary data

Supplementary data to this article can be found online at https://doi.org/10.1016/j.memsci.2022.120885.

## References

[1] Y.I. Kim, S.G. Kim, S.M. Kim, E.H. Kim, Y.K. Choi, Infection and rapid transmission of SARS-CoV-2 in ferrets, Cell Host Microbe 27 (5) (2020) 704–709, e2.
[2] A. Cvg, A. Dodb, A. Ai, B. Mt, B. Gk, C. Pema, A. Ifjv, Ultra-thin and highly porous PVDF-filters prepared via phase inversion for potential medical (COVID-19) and industrial use, J. Membr. Sci. 639 (2021), 119710.
[3] H. Huang, C. Fan, M. Li, H.L. Nie, J. Huang, COVID-19: a Call for physical scientists and engineers, ACS Nano 14 (4) (2020) 3747–3754.
[4] J.C. Prata, A. Silva, T.R. Walker, A.C. Duarte, T.R. Santos, COVID-19 pandemic repercussions on the use and management of plastics, Environ. Sci. Technol. 54 (13) (2020) 7760–7765.
[5] K.L. Xu, J.X. Deng, R. Lin, H. Zhang, Q.F. Ke, C. Huang, Surface fibrillation of para-aramid nonwoven as a multi-functional air filter with ultralow pressure drop, J. Mater. Chem. A. 8 (42) (2020) 22269–22279.
[6] Q.F. Wang, Y.Z. Wei, W.B. Li, X.Z. Luo, X.Y. Zhang, J.C. Di, G.Q. Wang, J.H. Yu, Polarity-dominated stable N97 respirators for airborne virus capture based on nanofibrous membranes, Angew. Chem., Int. Ed. 60 (44) (2021) 23756–23762.
[7] M. Shen, Z. Zeng, B. Song, H. Yi, R. Xiao, Neglected microplastics pollution in global COVID-19: disposable surgical masks, Sci. Total Environ. 790 (2021), 148130.
[8] Z. Peng, A. Rojas, E. Kropff, W. Bahnfleth, G. Buonanno, S.J. Dancer, J. Kurnitski, Y. Li, M. Loomans, L.C. Marr, Practical indicators for risk of aAirborne transmission in shared indoor environments and their application to COVID-19 outbreaks, Environ. Sci. Technol. 56 (2) (2022) 1125–1137.
[9] K. Pal, G.Z. Kyzas, S. Kralj, F. Souza, Sunlight sterilized, recyclable and super hydrophobic anti-COVID laser-induced graphene mask formulation for indelible usability, J. Mol. Struct. 1233 (4) (2021), 130100.
[10] S. Morgana, B. Casentini, S. Amalfitano, Uncovering the release of micro/nanoplastics from disposable face masks at times of COVID-19, J. Hazard. Mater. 419 (2021), 126507.
[11] T. Lu, J.X. Cui, Q.L. Qu, Y.L. Wang, J. Zhang, R.H. Xiong, W.J. Ma, C.B. Huang, Multistructured electrospun nanofibers for air filtration: a Review, Acs Appl. Mater. Inter. 13 (20) (2021) 23293–23313.
[12] J. Wen, X. Tan, Y. Hu, Q. Guo, X. Hong, Filtration and electrochemical disinfection performance of PAN/PANI/AgNWs-CC composite nanofiber membrane, Environ. Sci. Technol. 51 (11) (2000) 6395–6403.
[13] C. Jpcab, D. Scc, B. Xqw, C. Xxkb, B. Rxwa, C. Ymzab, Multilevel structured TPU/PS/PA-6 composite membrane for high-efficiency airborne particles capture: preparation, performance evaluation and mechanism insights, J. Membr. Sci. (2021), 119392.
[14] W. Deng, Y. Sun, X. Yao, K. Subramanian, S. Wang, Masks for COVID-19, Adv. Sci. 9 (2022), 2102189.
[15] S.S. Feng, Z.X. Zhong, Y. Wang, W.H. Xing, E. Drioli, Progress and perspectives in PTFE membrane: preparation, modification, and applications, J. Membr. Sci. 549 (2018) 332–349.
[16] Z. Wang, F. Yan, H.C. Pei, J.X. Li, Z.Y. Cui, B.Q. He, Antibacterial and environmentally friendly chitosan/polyvinyl alcohol blend membranes for air filtration, Carbohydr. Polym. 198 (2018) 241–248.
[17] N. El-Atab, N. Qaiser, H.S. Badghais H, S.F. Shaikh, M.M. Hussain, A flexible nanoporous template for the design and development of reusable anti-COVID-19 hydrophobic face masks, ACS Nano 14 (6) (2020) 7659–7665.
[18] J.P. Ruparelia, A.K. Chatteriee, S.P. Duttagupta, S. Mukherji, Strain specificity in antimicrobial activity of silver and copper nanoparticles, Acta Biomater. 4 (3) (2008) 707–716.
[19] C. Vishwasrao, B. Momin, L. Ananthanarayan, Green synthesis of silver nanoparticles using sapota fruit waste and evaluation of their antimicrobial activity, Waste Biomass Valorization 10 (8) (2019) 2353–2363.
[20] J. Ramyadevi, K. Jeyasubramanian, A. Marikani, G. Rajakumar, A.A. Rahuman, Synthesis and antimicrobial activity of copper nanoparticles, Mater. Lett. 71 (2012) 114–116.
[21] J.H. Jung, G.B. Hwang, J.E. Lee, G.N. Bae, Preparation of airborne Ag/CNT hybrid nanoparticles using an aerosol process and their application to antimicrobial air filtration, Langmuir 27 (16) (2011) 10256–10264.
[22] J. Choi, B.J. Yang, G.N. Bae, J.H. Jung, Herbal extract incorporated nanofiber fabricated by an electrospinning technique and its application to antimicrobial air filtration, Acs Appl. Mater. Inter. 7 (45) (2015) 25313–25320.
[23] A. Sahebkar, C. Serban, S. Ursoniu, M. Banach, Effect of curcuminoids on oxidative stress: a systematic review and meta-analysis of randomized controlled trials, J. Funct.Foods 18 (2015) 898–909.

[24] A. Tiwari, A. Singh, N. Garg, J.K. Randhawa, Curcumin encapsulated zeolitic imidazolate frameworks as stimuli responsive drug delivery system and their interaction with biomimetic environment, Sci. Rep. 7 (1) (2017), 12598.
[25] H. Soleimani, A. Amini, S. Taheri, E. Sajadi, S. Shafikhani, L.A. Schuger, V. B. Reddy, S.K. Ghoreishi, R. Pouriran, S. Chien, M. Bayat, The effect of combined photobiomodulation and curcumin on skin wound healing in type I diabetes in rats, J. Photochem. Photobiol., B 181 (2018) 23–30.
[26] C.V.B. Martins, D.L. da Silva, A.T.M. Neres, T.F.F. Magalhaes, G.A. Watanabe, L. V. Modolo, A.A. Sabino, A. de Fatima, M.A. de Resende, Curcumin as a promising antifungal of clinical interest, J. Antimicrob. Chemother. 63 (2) (2009) 337–339.
[27] B.K. Sahoo, K.S. Ghosh, S. Dasgupta, Investigating the binding of curcumin derivatives to bovine serum albumin, Biophys. Chem. 132 (2–3) (2008) 81–88.
[28] S.H. Mun, D.K. Joung, Y.S. Kim, O.H. Kang, S.B. Kim, Y.S. Seo, Y.C. Kim, D.S. Lee, D.W. Shin, K.T. Kweon, D.Y. Kwon, Synergistic antibacterial effect of curcumin against methicillin-resistant staphylococcus aureus, Phytomedicine 20 (8–9) (2013) 714–718.
[29] W.T. He, Z.X. Low, S.S. Feng, Q. Zhou, F. Zhang, Z.X. Zhong, W.H. Xing, Prediction and optimization of interlayer-interface resistance for expanded polytetrafluoroethylene-laminated polyphenylene sulfide composite membranes, Ind. Eng. Chem. Res. 61 (19) (2022) 6662–6672.
[30] M. Zhao, L. Liao, W. Xiao, X.Z. Yu, H.T. Wang, Q.Q. Wang, Y.L. Lin, F.S. Kilinc-Balci, A. Price, L. Chu, M.C. Chu, S. Chu, Y. Cui, Household materials selection for homemade cloth face coverings and their filtration efficiency enhancement with triboelectric charging, Nano Lett. 20 (7) (2020) 5544–5552.
[31] J.W. Wu, H.J. Zhou, J.Y. Zhou, X. Zhu, B.W. Zhang, S.S. Feng, Z.X. Zhong, L. X. Kong, W.H. Xing, Meltblown fabric vs nanofiber membrane, which is better for fabricating personal protective equipments, Chin. J. Chem. Eng. 36 (2021) 1–9.
[32] K. Chen, X.Q. Qiu, D.J. Yang, Y. Qian, Amino acid-functionalized polyampholytes as natural broad-spectrum antimicrobial agents for high-efficient personal protection, Green Chem. 22 (19) (2020) 6357–6371.
[33] X. Zhu, S. Feng, Y. Rao, S. Ju, Z. Zhong, W. Xing, A novel semi-dry method for rapidly synthesis ZnO nanorods on $SiO_2$ @PTFE nanofiber membrane for efficient air cleaning, J. Membr. Sci. 645 (2022), 120206.
[34] J. Xu, X. Xiao, W. Zhang, R. Xu, C.K. Sang, Y. Cui, T.T. Howard, E. Wu, Y. Cui, Air-filtering masks for respiratory protection from PM $_{2.5}$ and pandemic pathogens, One Earth 3 (5) (2020) 574–589.
[35] E.F. de Oliveira, J.V. Tosati, R.V. Tikekar, A.R. Monteiro, N. Nitin, Antimicrobial activity of curcumin in combination with light against Escherichia coli O157:H7 and Listeria innocua: applications for fresh produce sanitation, Postharvest Biol. Technol. 137 (2018) 86–94.
[36] L. Wang, J. Xue, Y. Zhang, Preparation and characterization of curcumin loaded caseinate/zein nanocomposite film using pH-driven method, Ind. Crop. Prod. 130 (2019) 71–80.
[37] Q.Y. Ma, L. Du, L.J. Wang, Tara gum/polyvinyl alcohol-based colorimetric NH3 indicator films incorporating curcumin for intelligent packaging, Sensor. Actuat. B-Chem. 244 (2017) 759–766.
[38] Z.M. Markovic, D.P. Kepic, D.M. Matijasevic, V.B. Pavlovic, S.P. Jovanovic, N. K. Stankovic, D.D. Milivojevic, Z. Spitalsky, I.D. Holclajtner-Antunovic, D.V. Bajuk-Bogdanovic, M.P. Niksic, B.M.T. Markovic, Ambient light induced antibacterial action of curcumin/graphene nanomesh hybrids, RSC Adv. 7 (57) (2017) 36081–36092.
[39] F.L. Yen, T.H. Wu, C.W. Tzeng, L.T. Lin, C.C. Lin, Curcumin nanoparticles improve the physicochemical properties of curcumin and effectively enhance its antioxidant and antihepatoma activities, J. Agric. Food Chem. 58 (12) (2010) 7376–7382.
[40] Y.K. Deng, T. Lu, J.X. Cui, W.J. Ma, Q.L. Qu, X.L. Zhang, Y.Y. Zhang, M.M. Zhu, R. H. Xiong, C.B. Huang, Morphology engineering processed nanofibrous membranes with secondary structure for high-performance air filtration, Separ. Purif. Technol. 294 (2022), 121093.
[41] J.W. Chen, Z.X. Low, S.S. Feng, Z.X. Zhong, W.H. Xing, H.T. Wang, Nanoarchitectonics for electrospun membranes with asymmetric wettability, Acs Appl. Mater. Inter. 13 (51) (2021) 60763–60788.
[42] A. Justin Kleingartner, Srinivasan, Truong Siddarth, T. Quoc, Sieber Michael, E. Robert Cohen, Designing robust hierarchically textured oleophobic fabrics, Langmuir 31 (48) (2015) 13201–13213.
[43] L. Li, X. Zhao, Z. Li, K. Song, COVID-19: performance study of microplastic inhalation risk posed by wearing masks, J. Hazard. Mater. 411 (6) (2020), 124955.
[44] R. Al-Attabi, Y. Morsi, J.A. Schutz, L.F. Dumee, One-pot synthesis of catalytic molybdenum based nanocomposite nano-fiber membranes for aerosol air remediation, Sci. Total Environ. 647 (2019) 725–733.
[45] G. Viswanathan, D.B. Kane, P.J. Lipowicz, High efficiency fine particulate filtration using carbon nanotube coatings, Adv. Mater. 16 (22) (2004) 2045–2049.
[46] Z.J. Dai, J. Zhu, J.Q. Yan, J.F. Su, Y.F. Gao, X. Zhang, Q.F. Ke, G.N. Parsons, An Advanced dual-function $MnO_2$-fabric air filter combining catalytic oxidation of formaldehyde and high-efficiency fine particulate matter removal, Adv. Funct. Mater. 30 (42) (2020), 2001488.
[47] Y. Bai, C.B. Han, C. He, G.Q. Gu, J.H. Nie, J.J. Shao, T.X. Xiao, C.R. Deng, Z. L. Wang, Washable multilayer triboelectric air filter for efficient particulate matter $PM_{2.5}$ removal, Adv. Funct. Mater. 28 (15) (2018), 1706680.
[48] L.A.T.W. Asri, M. Crismaru, S. Roest, Y. Chen, O. Ivashenko, P. Rudolf, J.C. Tiller, H.C. van der Mei, T.J.A. Loontjens, H.J. Busscher, A shape- adaptive, antibacterial-coating of immobilized quaternary- ammonium compounds tethered on hyperbranched polyurea and its mechanism of action, Adv. Funct. Mater. 24 (3) (2014) 346–355.
[49] X.L. Zhang, Q.L. Qu, W.X. Cheng, A.Y. Zhou, Y.K. Deng, W.J. Ma, M.M. Zhu, R. H. Xiong, C.B. Huang, A Prussian blue alginate microparticles platform based on gas-shearing strategy for antitumor and antibacterial therapy, Int. J. Biol. Macromol. 209 (2022) 794–800.
[50] S.Z. Moghadamtousi, H.A. Kadir, P. Hassandarvish, H. Tajik, S. Abubakar, K. Zandi, A review on antibacterial, antiviral, and antifungal activity of curcumin, Biomed Res. Int., 2014 (2014), 186864.
[51] D. Rai, J.K. Singh, N. Roy, D. Panda, Curcumin inhibits FtsZ assembly: an attractive mechanism for its antibacterial activity, Biochem. J. 410 (1) (2008) 147.
[52] Y. Li, J. Wang, Y. Liu, X. Luo, W. Lei, L. Xie, Antiviral and virucidal effects of curcumin on transmissible gastroenteritis virus in vitro, J. Gen. Virol. 101 (10) (2020) 1079–1084.
[53] B. Rattis, S.G. Ramos, M. Celes, Curcumin as a potential treatment for COVID-19, Front. Pharmacol. 12 (2021), 675287.